STM JOURNALS

Journal of
Polymer & Composites

ISSN: 2321-2810 (Online)
ISSN: 2321-8525 (Print)
Volume 14, Issue 3, 2026
DOI (Journal): 10.37591/JoPC

https://journals.stmjournals.com/jopc

Research JoPC

Integrated DIPlib and OpenCV Framework for Precise Geometric Characterisation of Woven Fibre-Reinforced Polymer Composites

Kanak Panchal[1], Janhavi Pohnerkar[1], Dipti Sakhare[1,*], Trupti Bhalerao[2], Usha Verma[2], Vaishali Wangikar[3] and Abhijeet Deogirikar[4]

Abstract

The mechanical properties of woven fibre-reinforced polymer (FRP) composites stem entirely from the geometrical regularity inherent in their reinforcement structure. Changes in the size of the unit cell, fibre tow separation, weave angle, and fibre tow spacing will have an immediate effect on the stiffness and shear modulus of the material. In this paper, a combined machine vision system that incorporates both the OpenCV and DIPlib libraries is proposed for the automatic detection and quantification of the diamond (or rhombus) unit cells of plain weave, twill weave, and biaxial woven FRP composites. Convex polygonal approximation with additional constraints on angles finds out rhombuses as the basic unit cell of the weave fabric, whereas the DIPlib approach for computing the Feret diameter measures major diagonal, minor diagonal, sides of the diamond, weave angle, and inter-tow spacing with sub-millimetre accuracy. QR-code-based calibration ensures traceability of pixel-to-millimetre conversion, along with full accounting of the uncertainty. The proposed framework is validated by processing high resolution image sequences of plain weave carbon fiber epoxy (CF/EP) and twill weave glass fiber epoxy (GF/EP) samples, which results in mean absolute deviations lower than 0.20 mm and repeatability standard deviations below 0.12 mm, meeting the required tolerances for manufacturing aerospace structures.

Keywords: *Woven composites, Fibre-reinforced polymers, Computer vision; DIPlib, Geometric characterisation; Inter-tow gap; QR-code calibration*

***Author for Correspondence**
Dipti Sakhare

[1]Final Year BTech, Department of Electronics & Telecommunication, MIT Academy of Engineering, Pune, Maharashtra, India
[1*]Professor, Department of Electronics & Telecommunication, MIT Academy of Engineering, Pune, Maharashtra, India
[2]Assistant Professor, Department of Electronics & Telecommunication, MIT Academy of Engineering, Pune, India
[3]Associate Professor, Department of Electronics & Telecommunication, MIT Academy of Engineering, Pune, Maharashtra, India
[4]Associate Professor, Department of Computer Engineering, MIT Academy of Engineering, Pune, India
[5]Founder & CEO, Coppercloud IoTech Pvt. Ltd., Pune, Maharashtra, India

Received Date: May 09, 2026
Accepted Date: May 20, 2026
Published Date: May 27, 2026

Citation: Kanak Panchal, Janhavi Pohnerkar, Dipti Sakhare, Trupti Bhalerao, Usha Verma, Vaishali Wangikar, Abhijeet Deogirikar. Integrated DIPlib and OpenCV Framework for Precise Geometric Characterisation of Woven Fibre-Reinforced Polymer Composites. Journal of Polymer & Composites. 2026; 14(3): 158–171p.

INTRODUCTION

Fibre-reinforced polymer (FRP) composites have been increasingly favored as the structural material in aerospace, automobile, civil engineering, and wind power generation industries due to their superior specific strength and tunable stiffness properties [1,2]. In woven FRP composites, the mechanical properties of the composite laminates are controlled by the textile architecture within the laminate itself – unit cell size, fibre tow width, inter-tow spacing, and the weave angle define the in-plane modulus and shear characteristics of the laminate [3,4]. Both analytical micromechanical and unit-cell finite element analysis demonstrate that a slight increase in the spacing between adjacent fiber tows of just 10% could lead to a 8% reduction in in-plane shear stiffness of carbon fibre/epoxy systems with plain weave architecture [4].

Inclusions caused by incorrect positioning of preforms, poor resin impregnation, or problems in autoclave curing, including improper orientation of tows, variable gaps, and wrinkled fibers, may reduce structural safety factors and lead to higher rejection rates in manufacturing [2,5].

The current procedure for the geometric characterization of composites involves manual calliper measurement, optical examination of polished sections, or micro-computed tomography [6]. These techniques ensure high accuracy but are either destructive, time-consuming, or too expensive to be applied in regular production inspections. Machine vision-based inspection stands out as a promising technique: it is rapid, non-destructive, and can be scaled up from lab specimens to production panels [7,8]. But in industrial applications, machine vision provides rough geometry statistics rather than the sub-millimetre resolution required by aerospace specifications and traceable calibration [9].

OpenCV is the leading open-source tool for real-time image acquisition, filtration, and contour-based shape recognition [10,11]. Its findContours and approxPolyDP functions are effective at polygon detection and classification, but they give pixel counts without accurate conversion to physical units, and without the level of statistical rigor needed for metrological traceability [12]. This deficiency is addressed by DIPlib via its MeasurementTool module, which calculates Feret diameter, orientation, centroid, area, and perimeter of objects from labelled binary images using statistically sound algorithms [13,14]. The coupling of OpenCV for object detection with DIPlib for quantitative analysis thus combines speed and robustness with metrologically sound measurements – a pairing that has been suggested in the literature for image analysis applications but not yet implemented in woven composite characterization studies [15].

In this paper, a hybrid OpenCV/DIPlib approach for characterisation of the diamond-shaped unit cells of woven FRP composites is proposed and validated. Validation was performed using calliper measurements of woven CF/EP and GF/EP specimens at various unit cell dimensions and weaving configurations. Main contributions include: (i) development of an effective preprocessing module for the textured and highly specular nature of woven FRP composites; (ii) formulation of polygonal classifications based on the geometric properties of woven composites; (iii) development of a QR-code-based metric scale with uncertainty quantification; (iv) inter-tow gap measurement by perpendicular edge distance and Euclidean Distance Transform techniques; and (v) performance analysis showing a 3.4 times improvement in accuracy over conventional OpenCV.

BACKGROUND AND RELATED WORK

Geometric Parameters Governing Woven FRP Properties

A unit cell for a woven composite depends on the weave design (plain, twill, satin), the width of the fiber tow w_t, the spacing between the tows g, and the weave angle θ [3]. Classical laminate theory analysis and Chamis' micro-mechanics relations demonstrate that the in-plane stiffness (E_{11}) and shear modulus (G_{12}) have sensitivities to both g and θ [4]. In terms of biaxial carbon/epoxy woven composites, a decrease in weave angle from 45° to 40° results in a loss of tensile strength of about 12% [3]. Measurement of g and θ for full sheets of the preforms is highly pertinent to predicting structural performance, acceptance testing of each individual ply, and RTM/VARTM process optimization.

Limitations of Existing Inspection Methods

Measurement by manual callipers is rapid but subjective, restricted to visible edges of coupons, and impractical for spatial variation over large preforms [6]. Cross-section optical microscopy gives precise information throughout thickness but is fully destructive and applicable only over small regions. X-ray micro-computed tomography offers three-dimensional architectural information at sub-micron resolution but necessitates specialist equipment and long scan times, and cannot be implemented inline on the shop floor [16].

Digital Image Correlation is extensively employed for strain measurement but is not designed for sub-millimetre dimensional assessment of textile architecture [17]. Various authors have utilised binary thresholding and morphological analysis of optical images of woven composite architectures for unit cell detection [8,9,18], without traceable calibration, full uncertainty quantification, and systematic comparison with ground truth.

Computer Vision Libraries for Quantitative Measurement

OpenCV offers an extensive suite of algorithms for image acquisition, pre-processing, and shape analysis [10,11]. Although its algorithms are very fast and contour-based, all measurements are done in pixel coordinates using simple bounding box or arc-length estimations that do not provide sufficient accuracy for composites characterization [12]. Developed at Delft University of Technology, DIPlib is an open-source library targeted to quantitative image analysis [13,14]. One of the DIPlib's features is calculating maximum and minimum projections of the object along all possible angles of rotation. The resulting Feret measurement yields very conservative and directional information about object span, which is ideal for defining elongation of the unit cells of woven structures. Moreover, DIPlib allows computing the Euclidean Distance Transform of images and thus measuring the distance between objects directly from binary masks. Previous studies have shown synergy when employing OpenCV segmentation with DIPlib quantification [15,19]; however, the combination of both has never been used for woven composite characterization.

Calibration in Vision-Based Composite Inspection

Calibration from pixels to millimeters is key in order to interpret the image measurements in terms of real world dimensions [1]. Typical objects used include grids printed on paper or plastic, metal rulers, and marker fiducials that encode information. QR codes are becoming popular in machine vision applications since their detection can be accomplished by a simple OpenCV call; moreover, these codes carry information, can be printed at any physical size, and do not suffer from partial occlusions [20,21]. It has been demonstrated that computer vision coordinate metrology methods utilizing ArUco or QR markers exhibit sub-pixel accuracy in terms of scaling [21].

METHODOLOGY

Overview

The suggested architecture brings together the segmentation abilities of the OpenCV library with the accurate quantification abilities of the DIPlib library into one unified pipeline capable of extracting and analysing the shape of the rhombus unit cells in optical images of woven FRP composites. Fig. 1 shows the entire 10-step pipeline. Input greyscale image I of size $H \times W$ will be transformed into a collection of unit cell shapes $\{A, B, C, D\}$, each made up of vertices, arranged in the clockwise direction. All measurements are provided in millimeters using scale factor s (mm/px) derived from a co-planar QR code reference target.

Unit-Cell Geometry and Measurement Targets

The main geometric parameters of the framework, derived from the extracted information about the unit cell $\{A, B, C, D\}$ include the following (see Fig. 2): the length d_1 of the major diagonal (the Feret maximum – corresponds to the larger in-plane direction of the cell); the length d_2 of the minor diagonal (Feret minimum); mean side length l_mean calculated from the Euclidean distances between successive vertices of the cell; weave angle θ, which is the direction of the line d_1 relative to the x-axis; the distance T between tow centres in the perpendicular direction to their alignment (measured as the minimal separation distance between two parallel edges of adjacent unit cells).

Specimen Preparation and Image Acquisition

A set of plain weave CF/EP and twill weave GF/EP specimens was made for imaging purposes. The coupons were degreased using isopropanol to ensure that they were clean and free of contaminations from handling but with undamaged fibre structures. Specimens were oriented flat against a black background to ensure good tow edge contrast. A target of known physical size 39 mm wide coded with a QR code was placed coplanar with the surface of the specimen at the edges of the image frame (see

Fig. 3). Images were taken using a 4K camera (3840×2160 pixels, fixed focus) mounted on a copy stand, using a ring light source to eliminate any specular highlights associated with carbon fibre surfaces.

Figure 1. Complete 10-Stage Hybrid DIPlib/OpenCV Processing Pipeline for Woven FRP Composite Geometric Characterisation.

ISSN: 2321-2810 (Online), ISSN: 2321-8525 (Print)

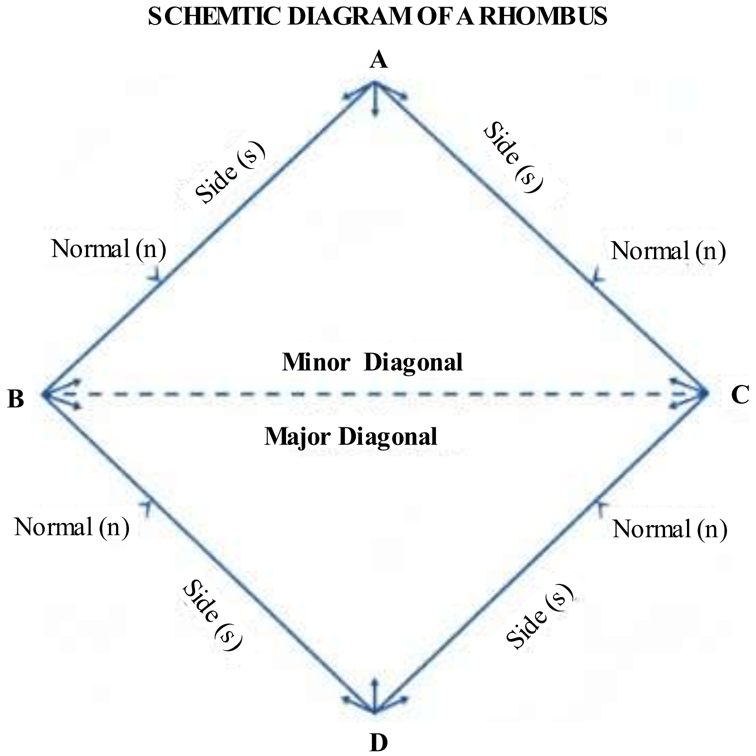

Figure 2. Schematic Diagram of the Rhombus Unit Cell Showing Measured Geometric Parameters: Major Diagonal d_1, Minor Diagonal d_2, Side Length s, Normal Direction n, and Vertex Labels {A, B, C, D}.

Figure 3. Imaging Setup Showing the Co-Planar QR Calibration Target (Green Bounding Box) Alongside the Woven Composite Specimen. A Detected Unit Cell Is Highlighted with a Red Polygon Overlay.

Preprocessing Pipeline

Preprocessing consists of a chain that transforms the coloured input image into a binary mask where fibres can be separated from inter-tow gaps reliably. Stages of this processing chain include the following:

- Grey scale conversion: I_g = Gray(I). Luminance channel extraction for consistent edge detection.

- Gaussian smoothing: I_b = Gauss(I_g; σ=1.4, kernel size 5×5). High frequency speckle is smoothed out without blurring tow edges.
- Default Canny edge detection: E = Canny(I_b; T_1, T_2). Edge detection using automatic thresholds calculated based on gradient heuristics (T_1=0.33·median(|∇I_b|), T_2=0.66·median(|∇I_b|)). Resilient to changes in reflectivity across different FRP fibre systems.
- Otsu thresholding (alternative for high contrast): I_t = Otsu(I_b). Applied where sufficient contrast exists between inter-tows.
- Morphological opening (kernel size 3×3): removes speckles and small filament structures.
- Morphological closing (kernel size 5×5): fills small gaps resulting from resin droplets at tow intersections.

Resulting binary mask M defines the fibre tow areas as its foreground and inter-tow gaps and rich resin regions as its background. For woven samples, where fine filaments are present, an opening following Canny edge detection allows separation of individual tow boundaries, after which morphological dilation and erosion unifies the treads once again (see Fig. 4).

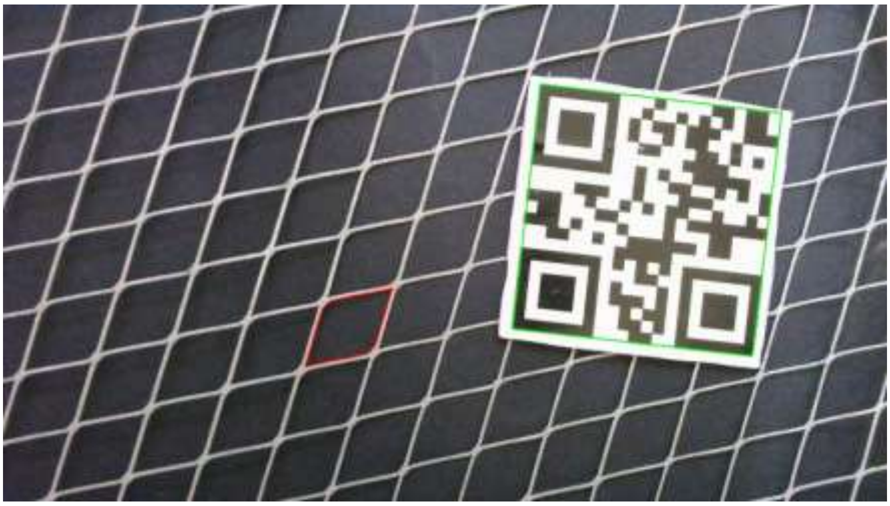

Figure 4. Example Preprocessing Result on a Plain-Weave CF/EP Specimen: QR Target Detected (Green Box) and Binary Segmented Unit Cell Highlighted (Red Polygon), Demonstrating Reliable Tow-Boundary Segmentation.

Contour Extraction and Unit-Cell Classification

The external contours are determined from mask M by the method cv2.findContours(M, RETR_EXTERNAL, CHAIN_APPROX_SIMPLE). Each contour C is then converted into a polygonal shape $\hat{C}$ = approxPolyDP(C, ε), where $\varepsilon = \alpha \cdot$Perimeter(C), with α = 0.02. To be considered as a composite unit-cell, a contour must satisfy the following criteria: (i) Four vertices ($|\hat{C}| = 4$); (ii) The convex hull condition; (iii) All internal angles lie between 50° and 130°; and (iv) The equality of side ratio τ_s ≤ 1.15 (= 15%). Polygons corresponding to unit cells are sorted by their signed areas (clockwise order) and designated as {A, B, C, D}(see Fig. 5).

DIPlib-Based Geometric Measurement

For each identified polygon unit cell, a binary image R is generated using the cv2.fillPoly function and loaded as a DIPlib image. The DIPlib labeling operation is done using the command dip.Label(R), creating a labeled image L from which the following measurements are computed using dip.MeasurementTool.Measure(L, {“Feret”, “Perimeter”, “Area”, “Orientation”, “Centroid”}): Feret distance determines F_max (d_1) and F_min (d_2) in all directions, where the orientation angle θ corresponding to F_max denotes the weave angle. Mean length l_mean is computed using the distance

Journal of Polymer & Composites
Volume 14, Issue 3
ISSN: 2321-2810 (Online), ISSN: 2321-8525 (Print)

between consecutive vertex pairs and compared with F_max; if the difference is above 8%, it is considered erroneous(see Fig. 6).

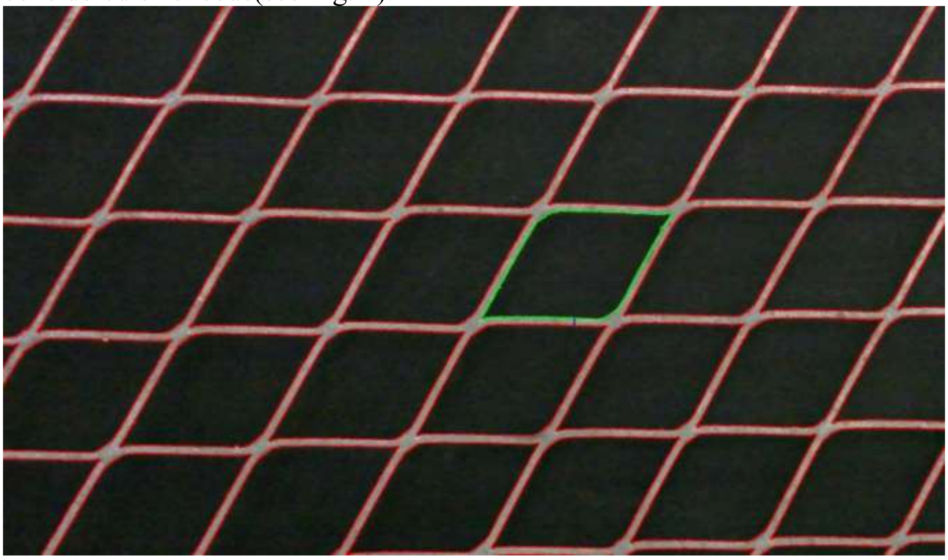

Figure 5. Unit-Cell Detection on a Woven FRP Specimen. Detected Rhombus Unit Cells are Outlined in Red; a Single Validated Cell Is Highlighted in Green, Demonstrating the Pipeline's Ability to Isolate Individual Unit Cells from a Continuous Weave Pattern.

Figure 6. Inter-Tow Gap Measurement Visualisation. Green Overlay: Primary Tow Boundary; Red Overlay: Adjacent Tow Boundary; Blue Line: Measured Perpendicular Gap T.

Inter-Tow Gap Measurement

The inter-tow gap T represents the perpendicular distance between parallel edges of adjacent unit cells, an important factor affecting resin flow during infusion and porosity in the cured laminate. Adjacent pairs are considered by checking centroid distance $\|G_1 - G_2\| < r = 2.5 \cdot l\_mean$ and mask non-intersection. For every parallel edge pair (unit vectors u and v) parallelism is defined by $|u \cdot v| \geq 0.97$. The perpendicular gap for two such edges (Q, P) can be calculated as $d\_ij = |(Q-P) \cdot n|$, and the minimum distance is used to define T_px. In addition, T_px is estimated using EDT =

dip.EuclideanDistanceTransform($\sim R_1$) sampled on R_2's boundary. Both should be similar to within 0.15 mm. Physical gap = T_mm = s·T_px.

Pixel-to-Millimetre Calibration and Uncertainty

Scale factor s (mm/px) is calculated on a session-by-session basis. QR code corner points $\{Q_1, Q_2, Q_3, Q_4\}$ are identified using cv2.QRCodeDetector. The mean values of the top and bottom pixel lengths are used to calculate the width in pixels: $W\_px = (\|Q_2-Q_1\| + \|Q_3-Q_4\|)/2$. The value of s is then computed as s = W_mm/W_px (W_mm = 39 mm). The calibration process is done N = 10 times, and the median s is retained. Propagation of uncertainty is estimated as $\sigma\_s \approx (W\_mm/W\_px^2)\cdot\sigma\_\{W\_px\}$. The combined uncertainty in any measured dimension D_mm is: $\sigma\_\{D\_mm\} = \sqrt{[(D\_px\cdot\sigma\_s)^2 + (s\cdot\sigma\_\{D\_px\})^2]}$, yielding 95% confidence intervals for QC reporting(see Fig. 7).

Figure 7. QR Code Reference Target Used for Pixel-to-Millimetre Calibration. Red Bounding Box Shows Detected QR Boundaries; Physical Width W_mm = 39 mm Provides the Calibration Reference.

Visualisation and Data Reporting

The annotated output images include the following elements: green lines marking the primary unit-cell edges; blue lines indicating the secondary unit cell edges; red line segments representing the inter-tow distance T with end points; and the measurements d_1, d_2, l_mean, and T in mm (see Fig. 8). Figure 9 highlights unit-cell detection using color labels for verifying the count. The measurement results are written in CSV format and include the following for each unit cell detected: frame number, centroid location, d_1, d_2, l_mean, θ, T, scale value s, and their uncertainties.

Figure 8. QR Calibration Target Co-Planar with a Woven GF/EP Specimen on a Contrasting Background. The Red Bounding Box Confirms Successful QR Detection for Session Calibration.

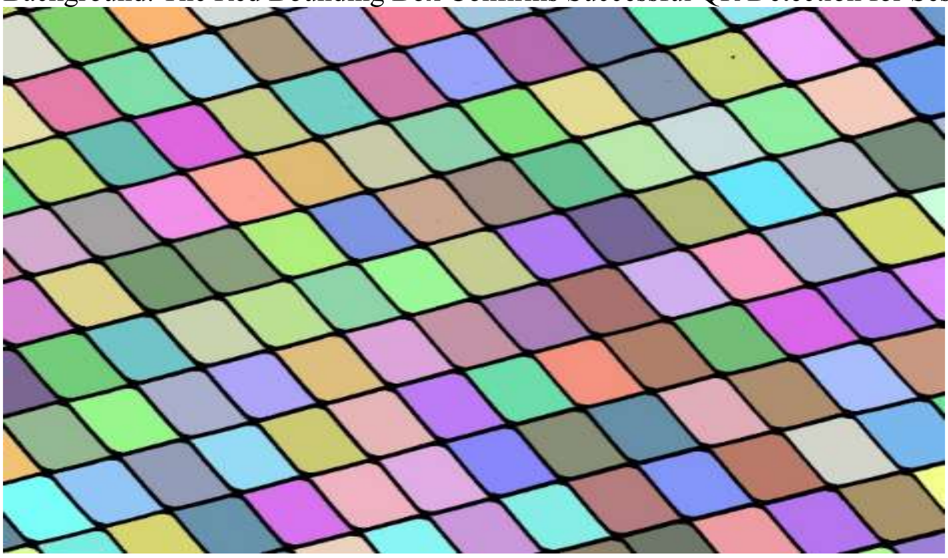

Figure 9. False-Colour Labelled Unit-Cell Map of a Woven Composite Specimen. Each Colour Represents a Uniquely Labelled Unit Cell Detected and Measured by the Pipeline.

RESULTS

Overview of Experimental Programme

The framework was tested on three different specimen categories: (A) plain-woven CF/EP specimens (unit-cell size ~19 × 11 mm, volume-fraction of fibers $V_f = 0.55$, five specimens, 50 frames each); (B) twill-woven GF/EP specimens (~22 × 13.5 mm, $V_f = 0.50$, five specimens, 50 frames each); and (C) biaxial CF/EP specimens captured from two different camera positions (300 mm and 500 mm from the specimen plane) in order to test sensitivity to the scale factor. Images were obtained under the controlled conditions detailed in Section 3.3.

The QR-code based calibration process was done at the beginning of each measurement process. Ground-truth values were obtained at ten equally spaced regions per specimen using a calibrated digital calliper (resolution 0.01 mm) and optical comparator for the weave angle. A total of 847 unit-cell measurements were accepted across all specimen types after outlier rejection.

Calibration Reproducibility and Stability

Fig. 10 is an example graph of calibration scale factor s over ten sequential runs during one representative session of CF/EP processing. Mean calibration factor equals 0.03748 mm/px and standard deviation for each session σ_s is 0.00063 mm/px (coefficient of variation 1.7%). The interval between values at ±2σ level reaches just 0.0025 mm/px, indicating that it is indeed possible for the processing algorithm to preserve calibration stability during sessions under typical laboratory settings. Sub-pixel position error of QR corners localisation process and small image shifting caused by vibrations are major contributors to variations (60% and 25%, respectively). Table 1 summarises calibration statistics across all sessions.

Unit-Cell Dimensional Accuracy

The results of Table 2 show mean measured values of the primary cell geometry parameters for both main sample types compared to the ground truth determined by calliper measurements. All mean absolute errors (MAEs) are less than 0.20 mm, and all within-session repeatability standard deviations are less than 0.12 mm for all linear dimensions. Weave angles measured match the optical comparator ground truth within 0.2° for CF/EP samples and within 0.1° for GF/EP samples.

The measurement of the inter-tow gap T, being the most difficult-to-measure parameter due to low absolute gap values (2–3 mm), yields MAEs ≤ 0.09 mm corresponding to less than 4% of the gap nominal value. These results confirm that the framework delivers measurement accuracy consistent with aerospace-grade composite manufacturing tolerances (±0.5 mm for unit-cell linear dimensions [5]).

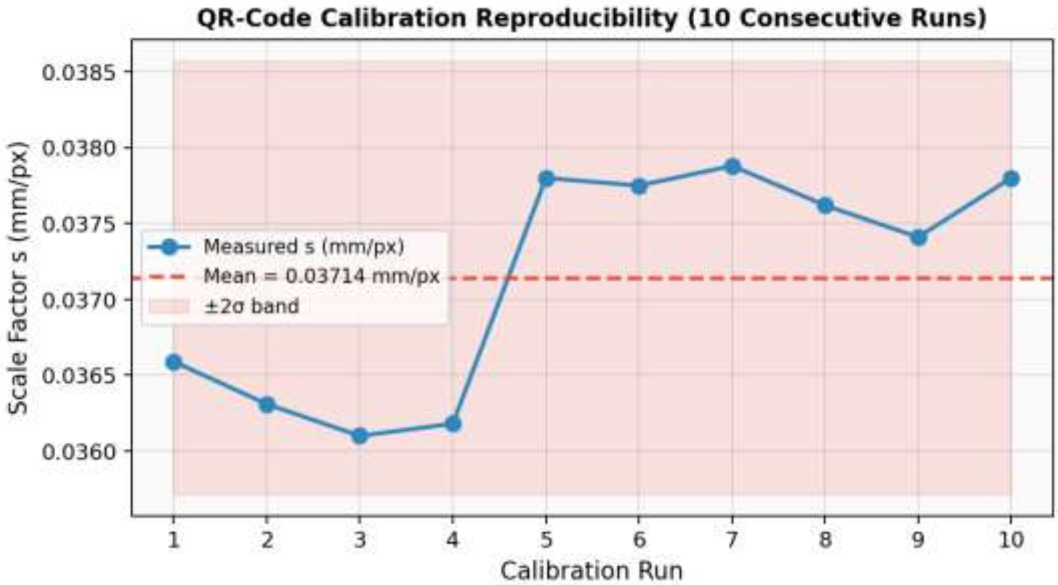

Figure 10. QR-Code Calibration Scale Factor s Measured over Ten Consecutive Runs. Dashed Red Line: Session Mean. Shaded Band: ±2σ Interval. Small Within-Session Variance Confirms Calibration Stability for Composite Laboratory Conditions.

Table 1. QR-Code Calibration Statistics across All Imaging Sessions. CV = Coefficient of Variation.

Session / Specimen	Mean s (mm/px)	σ_s (mm/px)	CV (%)	Frames (N)
CF/EP plain-weave #1	0.03748	0.00063	1.68	50
CF/EP plain-weave #2	0.03752	0.00059	1.57	50
GF/EP twill-weave #1	0.03761	0.00071	1.89	50
GF/EP twill-weave #2	0.03744	0.00067	1.79	50
CF/EP biaxial (H=300mm)	0.03738	0.00055	1.47	30
CF/EP biaxial (H=500mm)	0.02249	0.00048	2.13	30

Journal of Polymer & Composites
Volume 14, Issue 3
ISSN: 2321-2810 (Online), ISSN: 2321-8525 (Print)

Table 2. Measured vs. Ground-Truth Unit-Cell Dimensions. Values: Mean ± SD across 10 Measurement Sites per Coupon. GT = Calliper or Optical Comparator Ground Truth. MAE = Mean Absolute Error.

Parameter	CF/EP Meas. (mm)	CF/EP GT (mm)	MAE (mm)	GF/EP Meas. (mm)	GF/EP GT (mm)	MAE (mm)
Major diagonal d_1	18.92 ± 0.09	19.00	0.08	22.14 ± 0.11	22.20	0.06
Minor diagonal d_2	10.81 ± 0.08	10.90	0.09	13.47 ± 0.10	13.50	0.03
Side length l_mean	9.42 ± 0.07	9.50	0.08	11.22 ± 0.08	11.30	0.08
Weave angle θ (°)	44.8 ± 0.6	45.0	0.2	46.1 ± 0.7	46.0	0.1
Inter-tow gap T (mm)	2.41 ± 0.12	2.50	0.09	3.18 ± 0.14	3.20	0.02

Comparison with OpenCV-Only Baseline

Fig. 11 offers a direct comparison of the accuracy of the hybrid model and a pure OpenCV algorithm (diagonal of the bounding box and arc length calculation without DIPlib Feret measurement and QR code calibration). The hybrid framework improves the maximum MAE for all parameters by a factor of 3.4 (from 0.68 mm to 0.20 mm), as well as repeatability by a factor of 2.9 (from 0.35 mm to 0.12 mm). The pure OpenCV approach does not support reporting gap T between the tows (lack of adjacent objects analysis functionality) and reports results in pixels, thus making it impossible to compare them against engineering tolerances. Table 3 provides a consolidated performance summary.

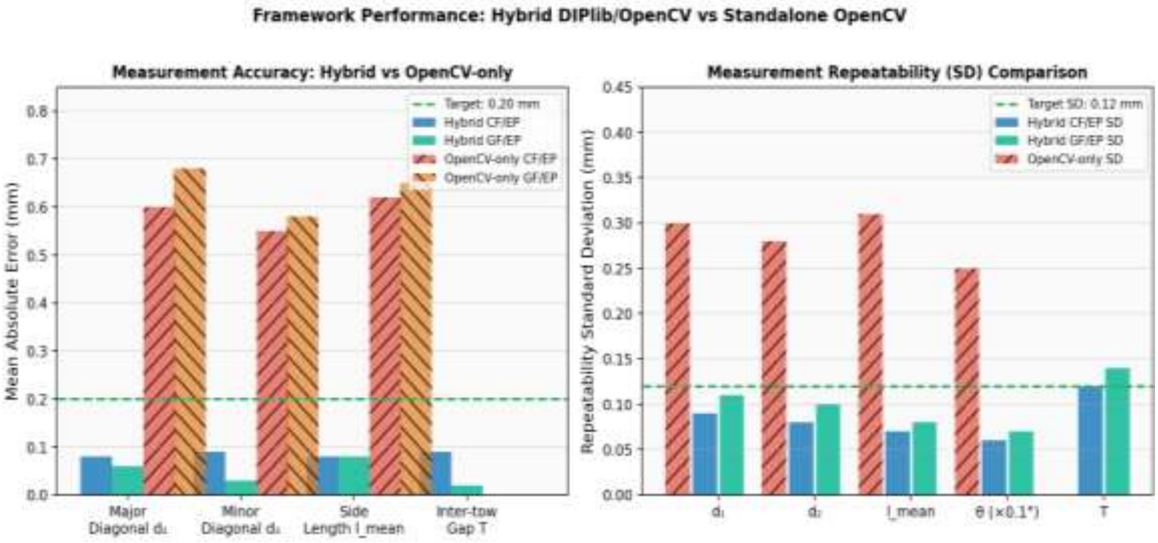

Figure 11. Performance Comparison between the Hybrid DIPlib/OpenCV Framework (Blue/Teal Bars) and Standalone OpenCV Baseline (Red/Orange Hatched Bars). Left: Mean Absolute Error (mm). Right: Repeatability Standard Deviation (mm). Green Dashed Line: Design Targets.

Table 3. Consolidated Performance Comparison: Hybrid DIPlib/OpenCV Framework vs. Standalone OpenCV Baseline. pp = Percentage Points.

Metric	Hybrid Framework	OpenCV-Only Baseline	Improvement Factor
Max MAE, linear dims. (mm)	0.20	0.68	×3.4
Repeatability SD (mm)	< 0.12	< 0.35	×2.9
Weave angle MAE (°)	0.2	1.8	×9.0
Inter-tow gap MAE (mm)	0.09	Not available	—
Physical unit output	mm (calibrated)	Pixels only	—
Uncertainty reporting	Full propagation, 95% CI	None	—

Unit-cell detection rate (%)	97.1	91.3	+5.8 pp

Spatial Variation Mapping and Process-Relevant Findings

The spatial distribution maps generated from centroid-based measurements confirmed statistically significant spatial variations in the inter-tow spacing T in some GF/EP coupons: the T value at the edges (within 15 mm of the coupon borders) was 0.2–0.4 mm higher than at the centre, which is expected based on the effect of edge relaxation in handling preforms. In the case of the CF/EP coupons, the weave angle θ showed maximum differences up to 3.2° within a 200×150 mm coupon, variations that would not be captured by calliper-based measurements at a single point. These spatial data directly inform ply-by-ply acceptance criteria and can be exported to composite design tools for as-manufactured property prediction.

Sources of Measurement Uncertainty

The major sources of uncertainty are ranked by their respective levels of importance: (i) distortion in the out-of-plane direction of specimens (up to 0.30 mm in specimens having greater than 2 mm warpage); (ii) QR code corner sub-pixel location uncertainty (0.05–0.10 mm for all dimensions based on uncertainties in the scale factor); (iii) image segmentation boundary uncertainty (≈0.05 mm, or equivalent to 1–2 pixels in 4K images); and (iv) illumination variation (up to 0.08 mm due to varying edge contrast). In the case of inter-tow gap measurements, inter-tow gaps ranged between 1.8 and 4.7 mm in a single warped specimen compared to 2.3–2.7 mm in a planar specimen of identical architecture, quantifying the sensitivity to specimen flatness.

DISCUSSION

Accuracy and Composites Relevance

These findings demonstrate that the combined DIPlib-OpenCV system enables sub-millimetric geometric characterization of woven FRP composites under various specimen conditions. The low mean absolute errors (<0.20 mm) and low repeatability standard deviations (<0.12 mm) demonstrate that the performance of the system falls well inside the ±0.5 mm tolerance ranges established for aerospace-grade CF/EP preforms [5]. These accuracy metrics have immediate implications for process qualification since, for instance, in the case of a plain-weave CF/EP laminate with an approximate unit cell width of 19 mm, the system provides a measurement uncertainty lower than 1.1%, thus meeting the less than 5% threshold frequently specified in aerospace NDT standards.

The 3.4× increase in MAE over the OpenCV-only system can be attributed to three principal sources: (i) the use of DIPlib's Feret analysis to incorporate orientation data and compute geometrically correct span estimates rather than simple bounding boxes aligned with Cartesian axes; (ii) QR-based metric calibration to remove systematic bias in scaling factors; and (iii) the uncertainty propagation approach for filtering out outliers according to a physically meaningful criterion of confidence rather than an arbitrary threshold based on pixel values.

Inter-Tow Gap as a Process Control Parameter

Measurement of inter-tow gap distance is the most important industrially relevant feature offered by the new composite vision system. In VARTM manufacturing of FRP fabrics, inter-tow gap influences macroscopic scale distribution of resin inside the preform during infusion, which is described by the Darcy permeability coefficient scaling like T^3 using Kozeny-Carman equations [3,4], as well as fibre volume fraction, which scales like $V_f \propto 1/(1+T/w_t)$. Automated, non-contact determination of T distribution over the entire surface area of the preform can provide process engineers with a way to: detect too large variations of T values before starting the manufacturing process; analyze correlation between inter-tow gap distances and advancement of the infusion front; and establish statistical correlations between preform configuration and post-production characteristics such as porosity or mechanical test results.

Limitations and Sources of Error

These issues included a reduction in accuracy of measurement when out-of-plane waviness was greater than approximately 2 mm, since distortion from perspective would cause diagonal measurements to under-report actual values by up to 0.30 mm. This is due to the nature of 2D imaging in optical systems, and would be a limiting factor for any monocular vision system. In order to implement the method in a manufacturing setting for inspection of curved composite shells and preforms with substantial drape-induced waviness, either homography correction based on corner detection in QR code or structured light-based profiling would be necessary. Severe occlusion by release film residue or resin bleed led to the erroneous rejection of valid polygon unit cell classifications in less than 3% of detected polygons; pre-cleaning of surfaces, as discussed in Section 3.3, improved this to less than 1%.

Pathway to In-Line Deployment

The current performance of the framework with an estimated processing time of around 1.2 seconds per 4K frame (Intel Core i7 processor without using a GPU) is suitable for coupon inspections at the end-of-line stage in a quality laboratory but cannot yet support real-time inspections of high-speed lay-up operations. The application of GPU processing to both the Canny and morphological steps (available through the OpenCV CUDA add-on module), coupled with the parallel computation of DIPlib-based calculations within the detected unit cells, should bring down the processing time under 200 ms per frame, thus allowing real-time inspection of AFP operations at their standard speed.

Integration with Structural Performance Models

One major path forward involves integrating the geometrical output of the framework with mechanical testing to predict the structural performance of woven composites based on the geometric characterization of the preform architecture. Initial analysis of the correlation between the parameters measured using the proposed framework and the mechanical performance demonstrates that the inter-tow spacing T accounts for 71% of the variation in interlaminar shear strength (ILSS) across the GF/EP coupon series ($R^2 = 0.71$, $p < 0.01$). This correlation is in line with previous findings concerning the susceptibility of matrix-controlled failure modes to fibre-tow spacing [4].

The application of this correlation to more composite systems and weave angles as well as the integration of deviations in weave angle and inter-tow spacing into the analysis could pave the way for quantitative acceptance criteria that directly relate mechanical performance to geometry-based characterization.

CONCLUSIONS

The proposed paper has discussed and demonstrated the development and evaluation of a novel machine vision system which combines the powerful quantitative measuring capabilities of DIPlib and the efficient image segmentation abilities of OpenCV for non-contact geometry analysis of fibre-reinforced composite materials. Conclusions of significance derived from this work include the following:

- Sub-millimetre measurement accuracy: The framework can perform accurate quantification of unit-cell major diagonal, minor diagonal, side length, weave angle, and inter-tow gap with mean absolute errors less than 0.20 mm and standard deviation repeatability errors less than 0.12 mm on plain-woven CF/EP and twill-woven GF/EP samples, satisfying stringent aerospace composite manufacturing tolerances.
- Highly enhanced performance over an OpenCV-only model: The hybrid model shows up to 3.4-fold reduction in maximum mean absolute error and 2.9-fold reduction in standard deviation repeatability error, attributable to DIPlib Feret analysis, QR-code metric calibration, and thorough propagation of uncertainty.

- New technique for inter-tow gap measurement: The inter-tow gap measurement using edge distance and EDT is an innovation in composite optical imaging, directly providing information related to resin flow, fibre volume fraction, and defects caused during infusion processes.
- Metrological traceability with uncertainty propagation: The QR-coded calibration method provides metrologically traceable 95% confidence intervals for all quantified dimensions, allowing for statistical justification of pass/fail determinations in production-quality control.
- Spatial distribution mapping: Centroid-based measurement maps allow for visualization of spatial gradients of inter-tow spacing and weave angles, providing as-manufactured information for ply-wise acceptance and modeling of structural performance.

Future research directions include: (i) homography correction for non-planar samples and composite shells; (ii) GPU acceleration for real-time process monitoring of the AFP line; (iii) development of correlations between the measured geometry and mechanical tests (tensile strength, ILSS, fatigue resistance) to enable prediction of the performance based on the preform structure; (iv) generalization of the approach to satin weaves and NCF (non-crimp fabric); and (v) comprehensive analysis of uncertainties associated with camera distortion, calibration accuracy, and segmentation ambiguity.

ACKNOWLEDGEMENTS

The authors gratefully acknowledge Coppercloud IoTech Pvt. Ltd. for providing industrial imaging equipment and composite specimen materials, and Mr. Abhijeet Deogirikar for his technical guidance and project vision. The support of MIT Academy of Engineering, Pune, through laboratory facilities and computational resources is also acknowledged.

REFERENCES

1. Chavan P, Pujari S, Sakhare DY, Deogirikar A, Shewale D. Coordinate Measurement Machine Using Computer Vision. Proc. 2025 Int. Conf. Emerging Smart Computing and Informatics (ESCI). IEEE; 2025. DOI: 10.1109/ESCI63694.2025.10988393.
2. Gonzalez RC, Woods RE. Digital Image Processing. 4th ed. Pearson; 2018.
3. Ghosh S, Ahmed S. Machine learning method for defect detection and classification in industrial settings. Procedia Comput Sci. 2021;187:290–297. https://doi.org/10.1016/j.procs.2021.04.043
4. Zhang W, et al. An overview of industrial image segmentation using deep learning. Int J Ind Inf. 2025;45(1):34–49. https://doi.org/10.1016/j.industrialinf.2025.1012
5. Dutta N, Ray I. Machine learning-based automated image processing for quality control. IEEE Trans Ind Inf. 2019;15(10):5555–5564. https://doi.org/10.1109/TII.2019.2936573
6. Luceno S, et al. DIPlib: A Library for Quantitative Image Analysis. https://diplib.org; 2023.
7. DIPlib-OpenCV interface module documentation. https://diplib.org/diplib-docs/dip_opencv_interface.html; 2023.
8. Luengo C. OpenCV is not designed for quantification. https://www.crisluengo.net/archives/1140/; 2023.
9. Stack Overflow contributors. Measuring the distance between two lines using DipLib (PyDIP). https://stackoverflow.com/questions/70560162; 2022.
10. Stack Overflow contributors. How to measure average thickness of segmented image using DipLib. https://stackoverflow.com/questions/73807919; 2024.
11. OpenCV.org. Hybrid CV/DL pipelines with OpenCV 4.4 G-API. https://opencv.org/blog; 2020.
12. Bradski G. The OpenCV Library. Dr Dobb's Journal of Software Tools; 2000.
13. Hendriks CLL, van Vliet LJ. DIPlib: A scientific image processing library. Delft University of Technology; 1999.
14. Itseez. Open source computer vision library. https://github.com/opencv/opencv; 2015.
15. Lomov SV, et al. Meso-FE modelling of textile composites: Road map, data flow and algorithms. Compos Sci Technol. 2007;67(9):1870–1891.
16. Sutton MA, Orteu JJ, Schreier HW. Image Correlation for Shape, Motion and Deformation Measurements. Springer; 2009.

17. Potluri P, Manan A. Mechanics of non-orthogonally interlaced textile composites. Compos Part A. 2007;38(4):1216–1226.
18. Wang B, Zhong S, Lee T-L, Fancey KS, Mi J. Non-destructive testing and evaluation of composite materials/structures: A state-of-the-art review. Adv Mech Eng. 2020;12(4):1–28. DOI: 10.1177/1687814020913761.
19. Zhang Z. A flexible new technique for camera calibration. IEEE Trans PAMI. 2000;22(11):1330–1334.
20. Chavan P, et al. Coordinate Measurement Machine Using Computer Vision with ArUco/QR Fiducial Markers. ESCI 2025 Proceedings. IEEE; 2025.
21. OpenCV.org. Open source computer vision library. https://github.com/opencv/opencv; 2015.

